Scanning electron microscopic, transmission electron microscopic, and confocal laser scanning microscopic observation of fibroblasts cultured on microgrooved surfaces of bulk titanium substrata

E. T. den Braber,[1] H. V. Jansen,[2] M. J. de Boer,[2] H. J. E. Croes,[3] M. Elwenspoek,[2] L. A. Ginsel,[3] J. A. Jansen[1]
[1]*Department of Biomaterials, University of Nijmegen, Dental School, POB 9101, NL-6500 HB Nijmegen, The Netherlands*
[2]*MESA Research Institute, Department of Electrical Engineering, University of Twente, POB 217, NL-7500 AE Enschede, The Netherlands*
[3]*Faculty of Medical Sciences, Department of Cell Biology and Histology, University of Nijmegen, POB 9101, NL-6500 HB Nijmegen, The Netherlands*

Received 30 December 1996; accepted 10 July 1997

Abstract: During this study, microtechnology and plasma etching were used to produce gratings 1.0 (TiD01), 2.0 (TiD02), 5.0 (TiD05), and 10.0 μm wide (TiD10) into commercially pure titanium wafers. After incubation of rat dermal fibroblast (RDFs) on these surfaces for 3 days, the cells were observed with scanning electron (SEM), transmission electron (TEM), and confocal laser scanning microscopy (CLSM). Results showed that the RDFs as a whole and their stress fibers oriented strictly parallel to the surface pattern on the TiD01 and TiD02 surfaces. On the TiD05 and TiD10 surfaces, this orientation was not observed. In addition, TEM and CLSM demonstrated that the focal adhesion points (FAP) were located mainly on the surface pattern ridges. TEM revealed that FAP were wrapped occasionally around the edges of the ridges. Only the RDFs on both the TiD05 and TiD10 surfaces protruded into the grooves and possessed FAP on the walls of the grooves. Attachment to the groove floor was observed only on the TiD10 textures. Comparison of these results with earlier observations on microtextured silicone rubber substrata suggests that material-specific properties do not influence the orientational effect of the surface texture on the observed RDF cellular behavior. The proliferation rate of the RDFs, however, seems to be much higher on titanium than on silicone rubber substrata. *J Biomed Mater Res,* **40,** 425–433, 1998.

Key words: surface topography; plasma etching; cellular orientation; focal adhesion point; *in vitro*

INTRODUCTION

Previous research has demonstrated that the response of cells and tissues to implant surfaces with micropatterns is unique and reproducible.[1–4] The results of these experiments have provided many investigators with the opportunity to hypothesize on the usefulness and advantages of textured implant surfaces over smooth ones.[1–4] For example, in an extensive review by Curtis and Clark[4] on this subject, some suggestions are summed up in favor of the application of surface micropatterns to medical devices, e.g.,

1. Reduction of lymphocyte penetration into grafted skin.
2. Improving nervous system regeneration—in particular, spinal cord regeneration.
3. Trapping cells such as tumor cells in topographical traps. Topographical traps in this case could be shapes that immobilize cells in certain positions.
4. Aligning and improving connective tissue and intracellular material.
5. Forming tubules of cells such as various ducts and capillaries.

Recognizing the possible potential of microtextured implant surfaces, many investigators have studied cellular behavior to various micropatterns produced in glass, polystyrene, silicon, quartz, Epon surface replicas, and silicone rubber surface replicas.[2,3–10] Although many silicone rubber implants do exist, other

Correspondence to: J. A. Jansen
Contract grant sponsor: Dutch Technology Foundation

 CCC 0021-9304/98/030425-09

materials such as titanium are usually used for implant purposes. However, until now this material was never applied in microtexturing experiments owing to difficulties of producing micropatterns in the surface of this metal. Some have tried to solve this problem by coating plasma-etched silicon surfaces with titanium.[10] However, although these studies have presented very useful results, this method offers no satisfactory solution for the fabrication of micropatterned titanium implant surfaces.

Therefore, the purposes of this study were (a) to investigate the possibility of producing micropatterns in bulk commercially pure titanium (cpTi), a frequently used biomaterial; and (b) to compare fibroblast behavior on these cpTi micropatterns with the results of our earlier experiments with microtextured silicone rubber substrata.

MATERIALS AND METHODS

Production and characterization of titanium microtextured wafers

To produce cell culture substrata, circular titanium wafers with a diameter of 76.2 mm (3 inches) were cut out of titanium plate material (cpTi Grade II; Engelhard-CLAL/Drijfhout B.V., The Netherlands). Subsequently, these cpTi wafers were polished mechanically (grit size $\geq$ 0.25 μm) to create a smooth surface, which is indispensable for accurate patterning with photolithography techniques.

Standard lift-off photolithography was used to transfer gratings 1.0, 2.0, 5.0, and 10.0 μm wide into Shipley 1805 photoresist. Before spinning the photoresist, the wafers were cleaned carefully in acetone and fuming 100% HNO_3 to remove particles and organic residues. After a prebake at 90°C, the titanium wafers were aligned and exposed using an ElectroVision Maskaligner. Finally, the exposed photoresist was removed in a Shipley developer (351), and a chromium layer of 50 nm was evaporated on the wafer surface as mask material by E-gun evaporation. Before plasma etching, the unexposed photoresist regions were removed by lift-off in an acetone ultrasonic bath.

After removal of the nonexposed chromium, SF_6/O_2 plasma-chemistry was used to etch the cpTi wafers with an ion energy of 250 eV in a standard RIE etcher (STS, PlasmaFab 340/310). Special precautions were taken to reduce the condensation of TiF_4 on the wafer surface and reactor wall. Therefore, the etch process was carried out at a pressure of 20 mTorr, while the chamber wall and electrode temperature were heated to a temperature of 80°C. After etching, the chromium layer was stripped off and the surface examined by scanning electron microscope (SEM; JEOL 6310), surface profilometer (DEKTAK 3030; Sloan), and energy-dispersive spectroscopy (EDS; Noran).

Cell culture

For harvesting rat dermal fibroblasts (RDFs), abdominal skin grafts were taken from male Wistar rats (100–120 g). After dissociation and culture of the RDFs as described earlier,[5–9] the fifth generation of these cells was identified as (myo)fibroblasts and used for further experiments.

Before using the cpTi wafers for cell culture purposes, these substrata were given an ultrasonic rinse in 30% nitric acid (Merck) for 5 min, followed by flushing the wafers with tapwater for 15 min. Subsequently, the substrata were rinsed ultrasonically in 20% Na_2CO_3 solution (15 min; Merck), dried under a constant N_2 gas flow, rinsed ultrasonically in pure acetone (Merck) for 5 min, and rinsed twice in distilled, deionized water for 15 min. Finally, the wafers were sterilized for cell culture by boiling in 70% ethanol for 15 min.

After air-drying the titanium wafers in a laminar flow cabinet and positioning them in the petri dishes ($\varnothing$ = 90 mm; Bibby Sterilin Ltd., UK), 2.0×10^5 viable RDFs in α-minimal essential medium (α-MEM) with Earl's salts and L-glutamine (Gibco), supplemented with 10% (v/v) heat-treated fetal calf serum (Gibco) were added to each wafer. The cells were incubated for 3 days (37°C, 5% CO_2–95% air) under static conditions, while growth medium was changed after 2 days of culture. These experiments were performed in sixfold.

Scanning electron microscopy (SEM) and transmission electron microscopy (TEM)

At the end of the incubation period, all cultures were given two 5-min rinses with phosphate-buffered saline (PBS) without magnesium and calcium (Dulbecco; pH 7.2) to remove nonattached cells. For SEM, the cells on the cpTi microgrooved substrata were fixed for 30 min with 2.5% glutaraldehyde 0.1*M* sodium cacodilate (pH 7.3), supplemented with 0.1*M* sucrose. After fixation, the wafers were rinsed twice with 0.1*M* phosphate buffer (30 min) and dehydrated using a graded ethanol series and tetramethylsilane (TMS) (5 min, Sigma).[11,12] Subsequently, the samples were air-dried, sputter-coated with gold, and viewed with SEM immediately after preparation.

For TEM, the cell cultures were treated as described before.[9] In short, the cells on the titanium wafers were fixed with 2.0% glutaraldehyde (Merck) in 0.1*M* phosphate buffer (pH 7.3) for 12 h at 4°C and postfixed with a 1.0% OsO_4 (Merck)–0.1*M* phosphate buffer solution for 1 h. Following dehydration with a graded ethanol series, random areas on the wafer were covered with Epon, which was left to polymerize for 24 h at 60°C. After polymerization, the Epon blocks were removed from the titanium surface by N_2 freeze fracture. These Epon blocks, which contained the RDFs and a cast of the microgrooved wafer surface, were reembedded in Epon. Ultrathin sections perpendicular to the surface grooves were cut on a Reichert OMU-3 ultramicrotome with a Diatome diamond knife. Sections were collected on Formvar-coated copper grids and stained with saturated uranylacetate (20 min) and lead citrate (10 min) for contrast enhancement. All specimens were observed with a JEOL 1010 transmission electron microscope.

Confocal laser scanning microscopy (CLSM)

Confocal laser scanning microscopic preparation and observation of the RDFs on the cpTi microgrooved wafers was

performed as described elsewhere.[8] In short, the titanium wafers were first rinsed with PBS to remove nonattached cells. After this first rinse, the cells were fixed with 2.0% paraformalin (Merck) in PBS for 15 min, and permeabilized with 1.0% Triton X-100 for 5 min. For visualizing the vinculin containing focal adhesion points of the RDFs, mouse monoclonal antibody hVIN-1 specific for vinculin[13] (30 min; Sigma) and fluorescein *iso*-thiocyanate (FITC)-conjugated goat anti-mouse immunoglobulin G (IgG) (30 min; Sigma) was used. The RDF stress fibers were visualized with thiorhodamine *iso*-thiocyanate (TRITC)-labeled phalloidin (30 min; Sigma).

Immediately after performing the double stains, the RDFs were viewed with a BioRad MRC 1000 CLSM (BioRad Laboratories). To avoid possible damage of the samples due to the size of the titanium wafers, the stained areas were not covered with a coverslip. Consequently, the CLSM consisted out of a Nikon Diaphot microscope with non–cover glass (NCG) objectives (Nikon). Next to the fluorescence mode, the krypton/argon mixed gas laser (Ion Laser Technology, Salt Lake City, UT) of the CLSM was used to visualize the underlying microtextured cpTi surface with the reflection mode. After storage of the digital images on 1-GB optical disk cartridges (LM-D702W, Panasonic), Confocal Assistant V3.10 for Windows™ 3.1× (available at ftp.genetics.biorad.com; copyright Todd Clark Brelje, 1995) was used to create 24 bits RGB (red-green-blue) overlay images. These digital images made it possible to capture the fluorescent and reflection data in one picture. The RGB images were transferred to CD-ROM by using a CD-ROM writer (CDD2000, Philips) for permanent storage and analysis.

RESULTS

Characterization of the microtextured wafer surfaces

Examination of the microtextured wafer surface with SEM showed some imperfections of the surface patterns. Frequently, dents (Fig. 1) and slopes (Fig. 2) in the wafer surface were seen, causing damage or discontinuity of surface ridges and the etched surface pattern in general. Occasionally, protrusions on the ridge edges were seen (Fig. 1). Further inspection revealed that the ridge crests were smooth, while the bottom of the grooves possessed an aspecific roughness. Finally, deviations of the ridge shape were observed. Although most ridges possessed a rectangular shape with angles close to 90°, the 1.0-μm ridges (TiD01) occasionally displayed a triangular configuration. In addition, some 5.0-μm (TiD05) and 10.0-μm (TiD10) ridge edges displayed signs of underetch, giving these surface features a mushroom-like appearance.

Concerning the dimensions of the surface patterns, the DEKTAK profilometer showed that the measured values differed from the intended designer values.

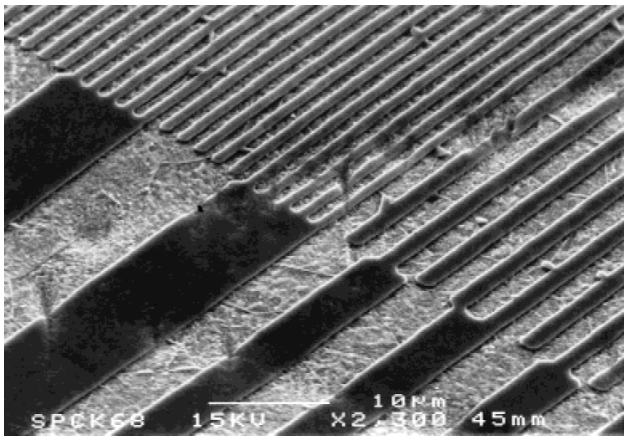

Figure 1. Scanning electron micrograph of four different microtextures on the cpTi wafer surfaces. The dents in the surface and consequential pattern damage are clearly visible. Furthermore, the protrusions on the surface edge and the difference in the roughness of the groove bottom and ridge crest can be seen.

The designer and actual surface texture dimensions can be found in Table I. Measurements also showed that the titanium wafers possessed a curvature of the surface. This curvature proved to be ≤0.09%, causing the depth of the surface grooves to range from 1.1 to 2.2 μm. Finally, EDS showed no chromium, natrium, or vanadium impurities of the titanium wafer surfaces.

SEM of the RDFs on the textured surfaces

Study of the RDFs on the microtextured cpTi surfaces with SEM showed large quantities of cells, which were arranged mainly as monolayers (Fig. 3). Occasionally, RDFs were seen on top of other cells (Fig. 4). This concerned single RDFs and not tightly packed,

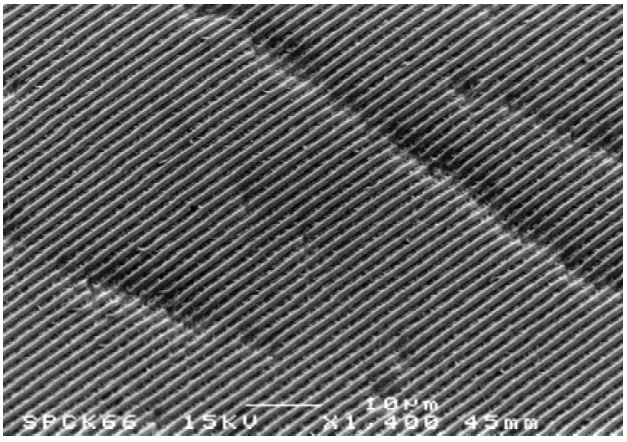

Figure 2. SEM image of a TiD01 surface. The slopes in the cpTi wafer surface cause imperfections of the etched surface pattern.

TABLE I
Designer and Measured Values of Micropatterns on Titanium Wafer Surfaces

Surface	Designer Values [Groove Width (μm)]	[Ridge Width (μm)]	Actual Values [Groove Width (μm)]	[Ridge Width (μm)]
TiD01	1.0	1.0	1.0	0.8
TiD02	2.0	2.0	2.1	1.4
TiD05	5.0	5.0	5.0	3.6
TiD10	10.0	10.0	9.2	8.0

continuous multilayers of cells. The majority of the RDFs on the textured surfaces had formed many cell–cell contacts (Fig. 3). These cell–cell contacts made the determination of the RDFs main direction of orientation difficult. Nevertheless, the main vector of orientation seemed to be directed parallel to the surface ridges on all patterns. This was especially clear on the TiD01, TiD02, and TiD05 surfaces.

Furthermore, we observed that all cells spanned the surface grooves, disregarding the groove width or depth (Fig. 3). Close examination of the RDF attachments frequently showed specific cell attachments to the surface ridges (Fig. 4) and other cells (Fig. 5) on all surface patterns. Distinct cell attachments to the bottom of the grooves could not detected by SEM.

TEM

General examination of the RDFs on the surfaces with TEM showed that these cells were arranged in a monolayer conformation. As with SEM, RDFs were seen occasionally on top of each other, but a continuous multilayer was not detected. Higher magnification demonstrated that all cells on all surfaces displayed a normal appearance (Figs. 6–10). The nucleus of the RDFs contained both euchromatin and heterochromatin, while in the cytosol, intracellular components such the endoplasmatic reticulum (ER), the Golgi apparatus, mitochondria lysosome, and autophage vacuoles were observed. Widening of the ER was not found in any of the cells. Ribosomes were seen either as free ribosomes or associated with the ER. Finally, small quantities of glycogen were observed in the cytosol.

Although the titanium wafers were removed during the preparation of the samples, an electron-dense film outlined the features on the surface of the removed wafer. This film, which was seen in all samples, was approximately 6 nm thick and probably consisted of adsorbed proteins originating from the culture medium. With the help of this film, it was possible to evaluate the quality of the etched surface features and the contact between these surface features and the RDFs.

Transmission electron microscopy confirmed that some areas of the TiD01 surfaces possessed triangular ridges (Fig. 6). RDFs on these triangular ridges contacted only the top of the ridges. Some focal adhesion points were found on the pointed ridges, but these structures were not defined as clearly as on the other surface patterns. No contact was found between the RDFs and the bottom of the TiD01 grooves.

The patterns on the TiD02 surfaces consisted solely of ridges with (near) rectangular edges (Fig. 7). Occasionally, electron-dense residues were seen, which

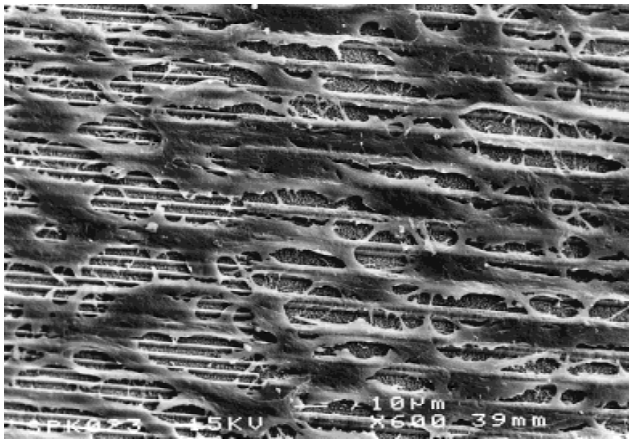

Figure 3. SEM photograph of RDFs on a TiD01 and TiD05 surface after 3 days of incubation. Although detection of the complete cell perimeter is difficult, the cells appear to be aligned parallel to the surface grooves and ridges.

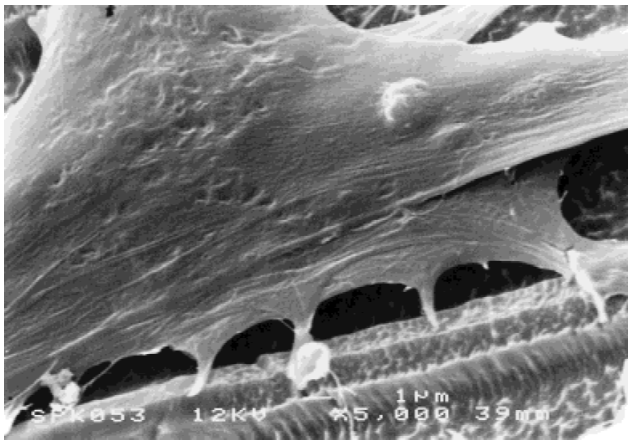

Figure 4. SEM image of two RDFs on a TiD02 surface after 3 days of incubation. Cell extensions of the bottom cell attach to the surface ridge.

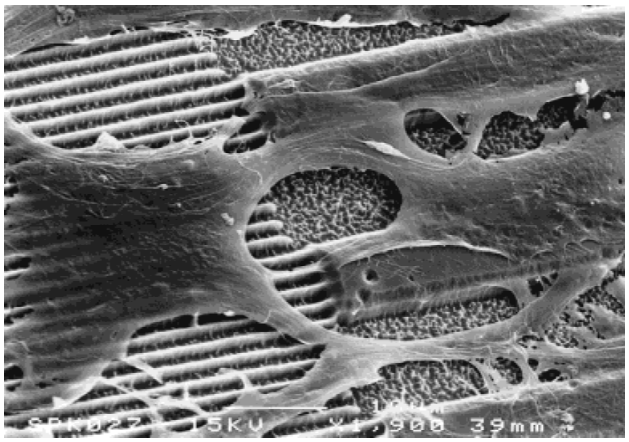

Figure 5. Scanning electron image of RDFs on a TiD01 and TiD10 surface after 3 days of incubation. The cells, which attach to the surface ridges or to each other through cell–cell contact, appear to avoid contact with the bottom of the grooves.

originated from the original titanium wafer surface. In contrast with the RDFs on the TiD01 surfaces, the cells on the TiD02 textures possessed many well-defined focal adhesion points. In none of the investigated TiD02 sections did RDFs contact the bottom of the surface grooves.

The ridges of the TiD05 patterns possessed protruding edges, which gave the ridges a mushroom-like shape (Figs. 8 and 9). Moreover, the angle between the walls and the floor of the surface grooves proved to be rounded. Although the RDFs on the TiD05 patterns protruded occasionally into the grooves, these cells never made contact with the floor of these grooves

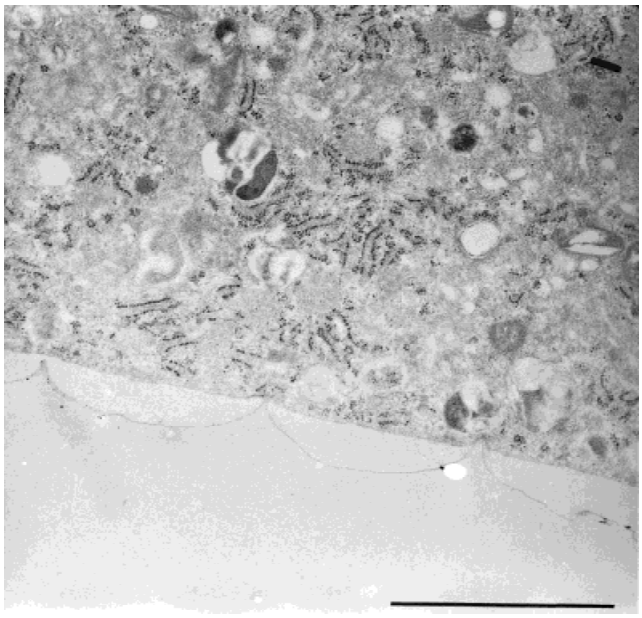

Figure 6. Transmission electron micrograph of an RDF on a TiD01 surface (bar = 1.0 μm; 3 days incubation). An electron-dense protein layer outlines the textured wafer surface. Despite the triangular surface ridges, the cell membrane appears not to be punctured. Focal contacts can be found at the points of contact between the cell and the surface ridges. No contact can be found between the cell and the bottom of the grooves.

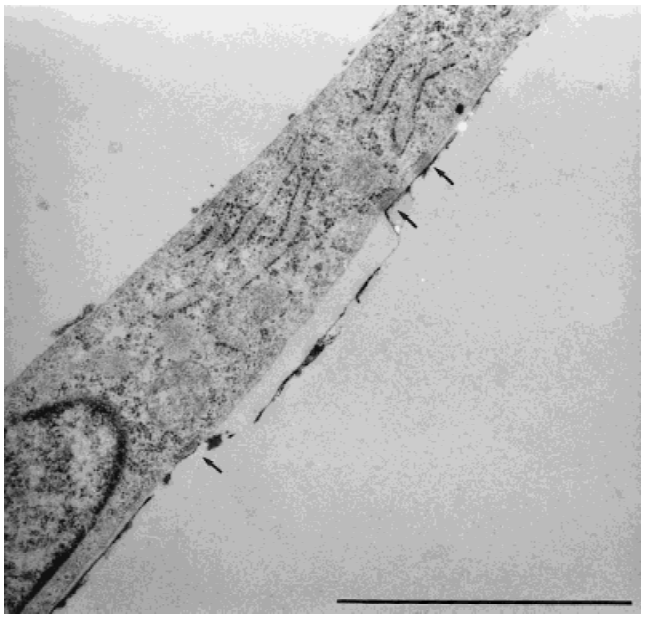

Figure 7. TEM micrograph of an RDF on a TiD02 surface (bar = 2.0 μm; 3 days incubation). Clearly defined focal adhesion points can be seen on or near the edges of the surface ridges. There is no contact between the RDF and the bottom of the groove. The electron-dense areas (arrows) are titanium residues torn off the wafer surface during TEM preparation.

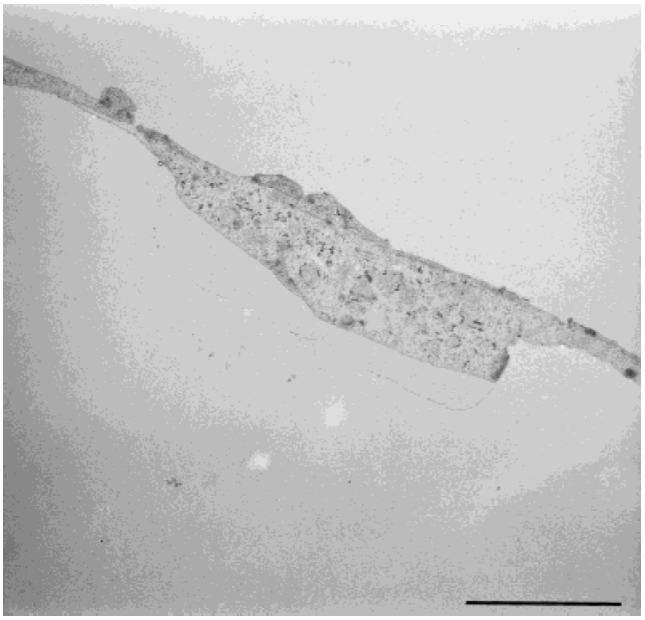

Figure 8. Transmission electron micrograph of an RDF on a TiD05 surface after 3 days of incubation (bar = 2.0 μm). The cell protrudes into the groove but does not contact the bottom of the groove. Focal adhesion points can be seen on the edge of the ridge and the wall of the surface groove.

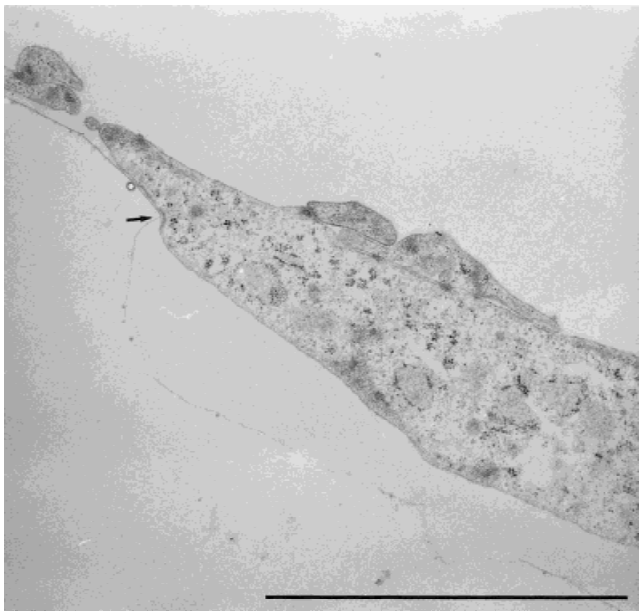

Figure 9. Higher TEM magnification of the RDF in Figure 10 (bar = 2.0 μm). A focal adhesion point (arrow) is wrapped around the edge of the surface ridge.

(Fig. 8). Focal adhesion points were found on the crests and edges of the ridges and on the walls of the surface grooves. Occasionally, these structures were wrapped around the edges of the ridges (Fig. 9).

Mushroom-shaped ridges and rounded angles between the groove wall and groove floor were also found with the TiD10 textures. Furthermore, the RDFs on these surface patterns also protruded into the surface grooves, but this occurred more frequently than on the TiD05 surfaces. At many sites, the cells on the TiD10 textures contacted the bottom of the grooves, often resulting in the formation of focal adhesion points (Fig. 10). In addition, the cells also showed the presence of focal adhesion points on the crests and edges of the ridges.

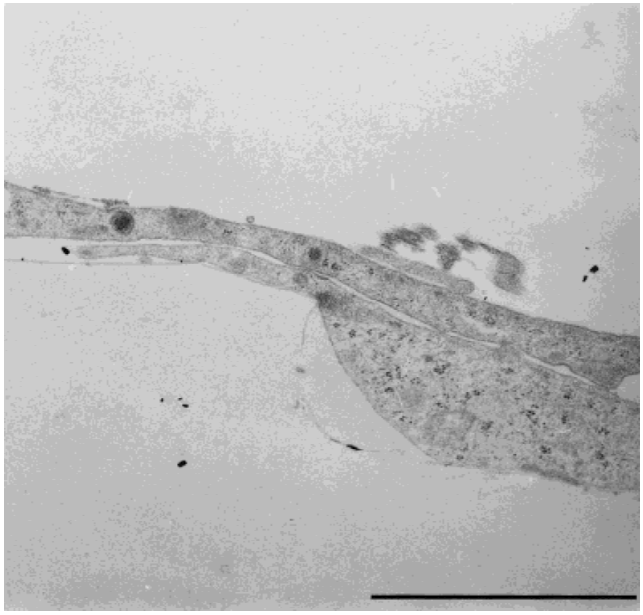

Figure 10. TEM image of RDFs on a TiD10 surface (bar = 2.0 μm; 3 days incubation). The underlying cell contacts and attaches to the bottom of the groove. Focal adhesion points are present on the edge of the ridge and the bottom of the groove.

CLSM

With the help of fluorescent staining techniques and additional imaging software, we studied the relation between the stress fibers, vinculin-containing attachment complexes, and the surface features. Careful examination of these digital images showed that the RDFs on the TiD01 and TiD02 surfaces possessed stress fibers that were highly aligned with the surface grooves and ridges (Fig. 11). Many of these fibers ended at the vinculin-containing focal adhesion points, which were located specifically on the surface ridges of these patterns. These focal points had an elongated ecliptic shape and were also oriented parallel with the surface ridges.

The predominant orientation of the stress fibers and vinculin-containing focal adhesion points was not observed on the TiD05 and TiD10 surfaces. On the TiD05 patterns, for example, a wide variety of highly oriented and nonoriented stress fibers was observed. The orientation of the vinculin-containing attachment complexes proved to be comparable with the orientation of the stress fibers which ended on these focal points (Fig. 12). In contrast with the TiD01 and TiD02 surfaces, vinculin on the TiD05 surfaces was oriented not only parallel, but also perpendicular to the surface

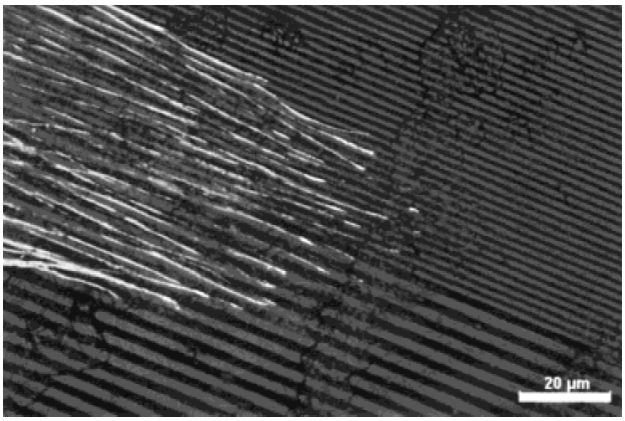

Figure 11. CLSM digital overlay image showing actin (red) and vinculin (green) and the cpTi surface (blue). Incubation lasted 3 days. On both the TiD01 (top) and the TiD02 (bottom) surface, the stress fibers and focal adhesion points are oriented parallel to the surface pattern. Vinculin is located mainly on the surface ridges.

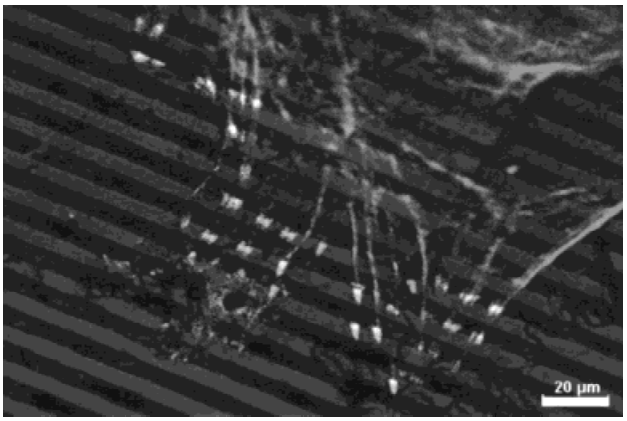

Figure 12. RGB overlay image of an RDF on a TiD05 surface (blue) after 3 days of incubation. The stress fibers (red) and focal adhesion points (green) are not oriented parallel to the surface grooves and ridges.

ridge (Fig. 12). Nevertheless, focal adhesion points were located on the surface ridges.

On the TiD10 surfaces, mainly nonoriented stress fibers and focal adhesion points were found. The differences in F-actin and vinculin orientation between different surface textures are demonstrated clearly in Figure 13. This CLSM image shows RDFs on a TiD01 and TiD10 surface texture. While the stress fibers and vinculin-containing focal adhesion points of the RDF on the TiD01 surface pattern were highly aligned, these intracellular components of the cells on the TiD10 texture were not. In contrast with the other surface patterns, some vinculin was found on the bottom of the 10.0-µm grooves. However, the majority of vinculin containing focal adhesion points were located on the crests of the TiD10 ridges.

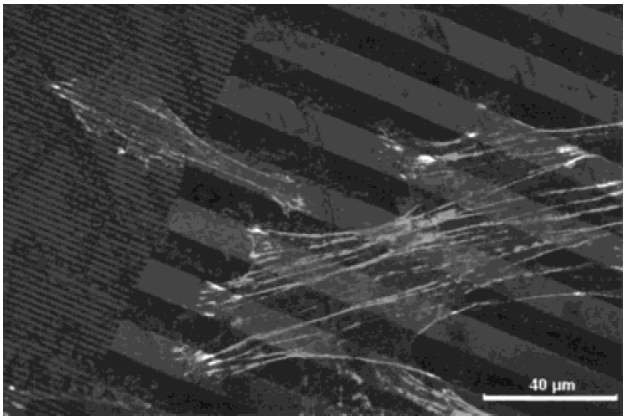

Figure 13. CLSM digital overlay image showing RDF F-actin (red), RDF vinculin (green), and the cpTi surface (blue). The image shows the transition from a TiD01 (left) to a TiD10 (right) texture. The cells were incubated for 3 days on these patterns. While the RDF on the TiD01 texture possesses highly aligned stress fibers and focal points, these intracellular components of the cell on the TiD10 surface are oriented differently.

DISCUSSION AND CONCLUSIONS

The results of this study show that it is possible to produce micropatterns in bulk commercially pure titanium. Although the quality of the micropatterns fell within set tolerance levels, results also made it clear that further minor adjustments will be required to optimize future cpTi microtextured surfaces. For instance, SEM showed dents, cavities, and slopes on the wafer surfaces. It is very likely that these features were remnants of damage inflicted when cutting the wafer to its appropriate size and shape, and during mechanical polishing of the wafer surface, the etching process, transport between laboratories, cell culture, or specimen preparation. A good example is the slopes (Fig. 2), whose appearance suggests that they originated as scratches which were reduced to slopes by polishing. The sharp-edged dents and cavities, on the other hand, imply damage after polishing. Although these surface imperfections were seen on a limited scale, their impact on the eventual patterns emphasizes the importance of continuous surface checks during the various stages of the production process.

Scanning electron microscopy and TEM showed that the 1.0-µm ridges had a triangular shape instead of a battlement-like appearance with rectangular edges. This could be caused by variations in the SF_6/O_2 etching process. During this process, a plasma is created by dissociating SF_6 in an RF field into SF_5^+ ions and F* radicals. While the SF_5^+ ions physically etch the bottom of the grooves through bombardment, the F* radicals chemically etch the walls and bottom of the grooves. In both cases, these processes result in the formation of TiF_4 gas, which is removed by maintaining a low-pressure environment in the reaction chamber. Introduction of O_2 offers the possibility of regulation, since the addition of O_2 facilitates the formation of a passivation layer which changes the etching speed. Next to variations during this etching process, the observed triangular ridges could also be due to the fact that the surfaces of the titanium wafers were not perfectly flat, but possessed a small curvature of 0.09%. A curved wafer surface could induce imperfections in the transferal of the designer patterned onto the photo-resist layer, resulting in deviations of the appearance of the eventual microfeatures. Except from the aberrant triangular ridge shapes, the observed deviations in groove width, ridge width, and groove depth could also be explained by the transferal and etching of gratings on nonplanar wafer surfaces.

In addition, SEM micrographs showed that the roughness of the floor of the grooves was clearly different from that of the crest of the ridges. This difference in roughness could be caused by the formation of TiO_3 instead of TiO_4 during the etching process. Since TiO_4 has a much lower sublimation point than TiO_3, it is possible that the latter was deposited on the groove

floor during etching, resulting in an specific rough surface. It is more likely, however, that this roughness was caused by the polycrystalline composition of the used cpTi wafers. Polycrystallinity is known to induce isotropic etching, since the molecule matrix of the material is oriented along several orientational planes. For this reason, most investigators prefer anisotropic materials such as silicon. However, these materials are not used for the production of implants. Therefore, further tuning of the etching process or perhaps the use of single-crystalline titanium seems to be a better option for enhancing the quality of etched micropatterns in titanium. Furthermore, subsequent etching of the wafer surface after removal of the protective chromium layer could produce a comparable roughness on both the groove floors and the ridge crests.

Concerning the behavior of the RDFs, SEM results suggested that the cells oriented parallel to the 1.0-, 2.0-, and 5.0-μm surface patterns, while the main direction of orientation of the RDFs on the TiD10 surfaces was very different. These results corroborate with our earlier studies with microtextured silicone rubber substrata.[5–7] During these earlier studies, digital image analysis showed that RDFs on silicone rubber surfaces with 2.0-μm grooves and ridges (SilD02) aligned strongly along the surface patterns, while the cells on the 5.0-μm grooves and ridges (SilD05) were less aligned. RDFs on silicone rubber substrata with 10.0-μm grooves and ridges (SilD10) proved to be oriented randomly.

Confocal laser scanning microscopy overlay images showed that the stress fibers of the cells on the TiD01 and TiD02 surfaces also were oriented strongly parallel to the surface ridges, while these fibers of the RDFs on the TiD05 and TiD10 patterns were not (Figs. 11 and 13). This again proved to be identical with the results of one of our earlier studies,[8] during which we found similar directional vectors for the microfilaments of the RDFs incubated on SilD02, SilD05, and SilD10 surfaces. Further similarities between the RDFs on microtextured cpTi and silicone rubber surfaces were found for the location and orientation of the vinculin containing focal adhesion points. On both the titanium and the silicone rubber surfaces, vinculin was located mainly on the ridges of the surface patterns. Furthermore, the orientation of these vinculin stains was highly comparable. On both the TiD02 and SilD02 surfaces, the vinculin stains were directed strictly parallel to the surface ridges, while on the TiD05, SilD05, TiD10, and SilD10 surfaces, other vinculin orientations were observed.

Similarities were also found for the TEM results. TEM showed that the RDFs on the TiD01, TiD02, and TiD05 surfaces did not touch the bottom of the grooves. This is in agreement with our findings on silicone rubber substrata[9] and earlier results by Rovensky and Slavnaya.[14] During our earlier TEM study,[9] we also found that the focal adhesion points of RDFs on microgrooved silicone rubber substrata were located mainly on the ridges. Again, comparable cell behavior was observed on the microgrooved titanium surfaces during this study. Finally, results showed that only the cells on the SilD10 and TiD10 textures contacted the floor of the grooves.

Recognizing the similarities between the results on the microtextured titanium and silicone rubber surfaces, it is possible to discuss the implications of these findings. For example, the physicochemical properties of silicone rubber and titanium are not identical. This, together with the role that these material properties play in cell attachment,[1–4,10] could cause the RDFs to orient differently on titanium. However, our results show that the alignment of the RDFs does not differ from that of RDFs on microtextured silicone rubber substrata.[5–9] The similarities could imply that the orienting effect of surface micropatterns is not influenced or overruled by material-related properties. However, this does not mean that the substratum material has no influence at all. This is demonstrated clearly by our SEM data, which show that large quantities of cells were found on the titanium surfaces after 3 days of culturing. Comparison with cell quantities on silicone rubber substrata[5–9] revealed that although identical amounts of RDFs were seeded (45 viable RDF/mm^2), fewer cells were present on these substrata after 3 days of incubation. This dissimilarity in cellular proliferation rate could be caused by differences in physicochemical properties of both substrata materials.[1,15] Material surface properties are considered crucial for cell adhesion and spreading,[1] cell activities that are related directly to the ability of fibroblasts to proliferate.[15] Therefore, it is possible to suggest that the more hydrophilic titanium surfaces induce a higher proliferation rate than the more hydrophobic silicon rubber surfaces.

Another point of attention is the effect of the difference in roughness between the crests of the ridges and the bottom of the grooves on the behavior of the RDFs. Earlier publications described that rough surfaces could elicit different behavior of cells if cultured on these surfaces. For example, Rich and Harris[16] found that fibroblasts avoided rough surfaces and preferred smooth ones. This behavior was termed ''rugophobia.'' In contrast, the fact that macrophages were seen to prefer rough surfaces over smooth ones was called ''rugophilia.'' With the results of the study of Rich and Harris in mind, it is possible to suppose that the rough surfaces of the floor of the grooves changed the behaviour of the RDFs. However, comparison with our earlier investigations with silicone rubber substrata showed similar results concerning the overall cellular orientation and the orientation of the intracellular components.[5–9] Whether the rough groove floors are able to induce rugophobia can be questioned, how-

ever. This is voiced by a publication of Ohara and Buck,[17] who stated that if the cells bridge the grooves, there will be no influence of the (depth of the) grooves. Since the TEM micrographs clearly show that the RDFs on the ≤5.0-μm gratings arch the grooves, this seems a valid opinion. However, whether the RDFs do not touch the bottom of the grooves because of rugophobia or because of another mechanism remains a subject for future research.

Finally, some remarks can be made concerning the focal adhesion points. TEM micrographs showed that the focal adhesion points were occasionally wrapped around the edges of the ridges, a phenomenon also observed by other investigators.[18,19] It is impossible to determine whether the detachment of the focal adhesion point shown in Figures 8 and 9 was caused by the histological procesures performed, without further dynamic time-dependent studies. However, the warped configuration of the shown focal adhesion points and the results of previous studies[18,19] clearly imply that these structures possess the ability to bend, and are therefore not rigid. This, together with the observed focal adhesion points on the walls of the ridges, seems to contradict with the hypothesis by Ohara and Buck,[17] which suggests that the geometrical dimensions of the focal adhesion points and the available area for attachment to the surface ridges are crucial elements in the process of cellular orientation. According to this theory, only one major orientational vector of attachment is possible on ridges with a width smaller than the minimum length required for focal adhesion point attachment, i.e., parallel to the surface grooves and ridges. Therefore, if the focal adhesion points are not rigid, cell attachment is not limited, for this reason. Subsequently, this would mean that other phenomena cause the cell to orientate and elongate on microgrooved surfaces.

References

1. A. F. von Recum and T. G. van Kooten, ''The influence of micro-topography on cellular response and the implications for silicone implants,'' *J. Biomater. Sci. Polym. Edn.,* **7,** 181–198 (1995).
2. R. Singhvi, G. Stephanopoulos, and D. I. C. Wang, ''Review: Effects of substratum morphology on cell physiology,'' *Biotechnol. Bioeng.,* **43,** 764–771 (1994).
3. D. M. Brunette, ''Effects of surface topography of implant materials on cell behavior in vitro and in vivo,'' in *Nanofabrication and Biosystems,* H. C. Hoch, L. W. Jelinski, and H. G. Craighead (eds.), Cambridge University Press, Cambridge, 1996, pp. 335–355.
4. A. S. G. Curtis and P. Clark, ''The effects of topographic and mechanical properties of materials on cell behavior,'' *Crit. Rev. Biocompat.,* **5,** 344–362 (1990).
5. E. T. den Braber, J. E. de Ruijter, H. T. J. Smits, L. A. Ginsel, A. F. von Recum, and J. A. Jansen, ''Effect of parallel surface micro grooves and surface energy on cell growth,'' *J. Biomed. Mater. Res.,* **12,** 511–518 (1995).
6. E. T. den Braber, J. E. de Ruijter, L. A. Ginsel, A. F. von Recum, and J. A. Jansen, ''Quantitative analysis of cell proliferation and orientation on substrata with uniform parallel surface micro grooves,'' *Biomaterials,* **17,** 1093–1099 (1996).
7. E. T. den Braber, J. E. de Ruijter, H. T. J. Smits, L. A. Ginsel, A. F. von Recum, and J. A. Jansen, ''Quantitative analysis of fibroblast morphology on microgrooved surfaces with various groove and ridge dimensions,'' *Biomaterials,* **17,** 2037–2044 (1996).
8. E. T. den Braber, J. E. de Ruijter, L. A. Ginsel, A. F. von Recum, and J. A. Jansen, ''Orientation of ECM protein deposition, fibroblast cytoskeleton, and attachment complex components on silicone microgrooved surfaces,'' *J. Biomed. Mater. Res.,* **40,** 291–300 (1998).
9. E. T. den Braber, J. E. de Ruijter, H. J. E. Croes, L. A. Ginsel, and J. A. Jansen, ''Transmission electron microscopical study of fibroblast attachment to microtextured silicone rubber surfaces,'' *Cells Mater.,* to appear.
10. B. Chehroudi and D. M. Brunette, ''Effects of surface topography on cell behavior,'' in *Encyclopedic Handbook of Biomaterials and Bioengineering,* D. L. Wise, D. J. Trantolo, D. E. Altobelli, M. J. Yaszemski, J. D. Gresser, and E. R. Schwartz (eds.), Marcel Dekker, New York, 1995, pp. 813–842.
11. W. J. Reville and M. P. Cotter, ''An evaluation of the usefulness of air-drying biological samples from tetramethylsilane in preparation for scanning electron microscopy,'' *J. Electron Microsc.,* **40,** 198–202 (1991).
12. S. Dey, T. S. Basu Baul, and B. Roy, ''A new rapid method of air-drying for scanning electron microscopy using tetramethylsilane,'' *J. Microsc.,* **156,** 259–261 (1989).
13. R. Benori, D. Salomon, and B. Geiger, ''Identification of two distinct domains on vinculin involved in its association with focal contacts,'' *J. Cell. Biol.,* **108,** 2383–2393 (1989).
14. Y. A. Rovensky and I. L. Slavnaya, ''Spreading of fibroblast-like cells on grooved surfaces,'' *Exp. Cell Res.,* **84,** 199–206 (1974).
15. T. Groth and G. Altankov, ''Studies on cell-biomaterial interaction: Role of tyrosine phosphorylation during fibroblast spreading on surfaces varying in wettability,'' *Biomaterials,* **17,** 1227–1234 (1996).
16. A. M. Rich and A. K. Harris, ''Anomalous preferences of cultured macrophages for hydrophobic and roughened surfaces,'' *J. Cell Sci.,* **50,** 1–7 (1981).
17. P. T. Ohara and R. C. Buck, ''Contact guidance in vitro,'' *Exp. Cell. Res.,* **121,** 235–249 (1979).
18. G. A. Dunn and A. F. Brown, ''Alignment of fibroblasts on grooved surfaces described by a simple geometric transformation,'' *J. Cell Sci.,* **83,** 313–340 (1986).
19. C. Oakley and D. M. Brunette, ''The sequence of alignment of microtubules, focal contacts and actin filaments in fibroblasts spreading on smooth and grooved titanium substrata,'' *J. Cell Sci.,* **106,** 343–354 (1993).